Statistics of avalanches in martensitic transformations. II. Modeling

Ismael Ràfols and Eduard Vives
Departament d'Estructura i Constituents de la Matèria, Facultat de Física, Universitat de Barcelona, Diagonal 647, E-08028 Barcelona, Catalonia, Spain
(Received 16 May 1995)

Using a scaling assumption, we propose a phenomenological model aimed to describe the joint probability distribution of two magnitudes A and T characterizing the spatial and temporal scales of a set of avalanches. The model also describes the correlation function of a sequence of such avalanches. As an example we study the joint distribution of amplitudes and durations of the acoustic emission signals observed in martensitic transformations [Vives *et al.*, preceding paper, Phys. Rev. B **52**, 12 644 (1995)].

I. INTRODUCTION

The study of avalanches has received an increasing attention during the last years, since the appearance of the ideas on self-organized criticality.[1] A large number of experiments has been performed in order to analyze the statistical properties of avalanches in a great variety of systems ranging from earth crust[2] to superconducting thin films.[3] Most of the studies have been devoted to demonstrating the absence of intrinsic temporal and spatial scales in the systems, reflected in power-law statistical distributions of different magnitudes. Concerning the spatial scales, although the size (volume, area or length) is difficult to measure directly, it has been possible to measure changes in related magnitudes like magnetization (for magnetic materials),[4,5] mass (in sandpiles),[6,7] acoustic emission (related to the avalanche advance),[8,9] resistance (in superconducting films),[3] and capacitance (in hysteretic capillary condensation).[10] On the other hand, concerning the temporal scales, both the duration of the avalanches and the waiting times between them have been experimentally investigated. A number of these experiments have also shown the existence of $1/f$-like noise arising from the distribution of the avalanches.

In this paper we provide a general mathematical framework for experiments simultaneously measuring two magnitudes of the avalanches, characterizing their spatial scale (A) and duration (T). The phenomenological model we are proposing will be applied, as an example, to recent measurements on acoustic emission (AE) in martensitic transformations (part I). The main goal is to describe the avalanches in terms of the joint probability distribution $p(A,T)$. This represents a step forward from the standard analysis of the marginal distributions $p(A)\sim A^{-\alpha}$ and $p(T)\sim T^{-\tau}$ allowing the measurement of the exponents α and τ. Our model for the joint probability distribution characterizes unambiguously the relation between A and T which is determined by the exponent x ($A\sim T^x$). The model, together with an hypothesis on the shape of the signal associated with each avalanche, also enables a correct description of the time correlation function and its power spectrum. It should be mentioned that a first model for a joint probability $p(A,T)$ was used in the study of the Barkhausen effect in ferromagnetic metals,[5] but it was restricted to find the relation between the marginal distributions and the power spectrum as proposed by Christensen *et al.*[11]

II. DISTRIBUTION FUNCTION MODELING

Let us consider the joint probability density $p(A,T)\ dA\ dT$ describing the probability of having a signal with an amplitude within A and $A+dA$ and a duration within T and $T+dT$. The two marginal probability densities are given by

$$p(A)=\int_{T_{\min}}^{T_{\max}} p(A,T)\ dT\ , \tag{1}$$

$$p(T)=\int_{A_{\min}}^{A_{\max}} p(A,T)\ dA\ , \tag{2}$$

where $T_{\max}$, $T_{\min}$, $A_{\max}$, and $A_{\min}$ are the upper and lower cutoffs for T and A imposed by each particular experimental setup and within which $p(A,T)$ is normalized, i.e.,

$$\int_{A_{\min}}^{A_{\max}}\int_{T_{\min}}^{T_{\max}} p(A,T)\ dA\ dT=1\ . \tag{3}$$

We are concerned with the study of a joint probability distribution leading to marginal power-law distributions:

$$p(A)\sim A^{-\alpha}\ , \tag{4}$$

$$p(T)\sim T^{-\tau}\ . \tag{5}$$

We propose the general scaling form

$$p(A,T)=g(A/T^x)A^{\gamma}f_T(T)\ , \tag{6}$$

with the function $g(Z)$ being a "well-localized" distribution function with a maximum around Z_0 and strongly decaying for higher or lower values of Z. The scaling with the variable $Z=A/T^x$ provides a precise definition of the exponent x. The functions g and f_T can always be redefined so that $p(A,T)=g^*(A/T^x)f_T^*(T)$. In this case, the marginal distribution for T would be

$$p(T)=\int_{A_{\min}}^{A_{\max}} p(A,T)\ dA=\int_{A_{\min}}^{A_{\max}} g^*(A/T^x)\ \ f_T^*(T)\ dA\ \ , \tag{7}$$

which, under the change $A\rightarrow Z=A/T^x$ reads

$$p(T)=f_T^*(T)\ \ T^x\int_{A_{\min}/T^x}^{A_{\max}/T^x} g^*(Z)\ dZ\ \ . \tag{8}$$

Under the assumption that $g(Z)$ is a well-localized function, the integral in (8) is a constant, independent of T, provided that $(A_{\min}/Z_0)^{1/x}\ll T\ll(A_{\max}/Z_0)^{1/x}$. By comparison with the power-law assumption for $p(T)$ [Eq. (5)] one gets $f_T^*(T)\sim T^{-\tau-x}$. Now, the marginal distribution $p(A)$ can be calculated as:

$$p(A)=\int_{T_{\min}}^{T_{\max}} p(A,T)\ dT=\int_{T_{\min}}^{T_{\max}} g^*(A/T^x)\ \ T^{-\tau-x}\ dT\ \ . \tag{9}$$

The change of variable $T\rightarrow Z=A/T^x$ leads to the desired power-law dependence $p(A)\sim A^{-\alpha}$, and to the exponent relation

$$x(\alpha-1)=(\tau-1)\ \ . \tag{10}$$

Straightforwardly, from the definition of f_T^* one gets $f_T(T)\sim T^{\delta}$ and the following exponent relations:

$$\alpha=-\frac{1}{x}(\delta+1)-\gamma\ \ , \tag{11}$$

$$\tau=-x(\gamma+1)-\delta\ \ . \tag{12}$$

Among the three equations (10), (11), and (12), only two of them are independent. By symmetry arguments, the same result can be obtained under the assumption $p(A,T)=g(A/T^x)f_A(A)T^{\delta}$ and imposing (4). Thus, the most general joint distribution with power-law marginal distributions that displays a $A\sim T^x$ dependence has been found to be

$$p(A,T)=g(A/T^x)\ \ A^{\gamma}\ \ T^{\delta}\ \ , \tag{13}$$

where, in principle, there is a degree of freedom in choosing the function g, and the exponents γ and δ. Such freedom will disappear on choosing a function g depending on a few parameters, like a Gaussian or a similar shaped function.

A two-dimensional (2D) histogram of such probability distribution will exhibit a crest between the two lines defined by $\partial p/\partial A=0$ and $\partial p/\partial T=0$ giving the two conditions

$$\frac{\partial p}{\partial A}=0\quad\Rightarrow\quad\frac{\partial\ \lg(Z)}{\partial\ \ln Z}=-\gamma\ \ , \tag{14}$$

$$\frac{\partial p}{\partial T}=0\quad\Rightarrow\quad\frac{\partial\ \lg(Z)}{\partial\ \ln Z}=\frac{\delta}{x}\ \ . \tag{15}$$

In a ln(T) vs ln(A) map, these two last equations correspond to two parallel straight lines with slope x, defined by $A/T^x=Z_A$ and $A/T^x=Z_T$. In Fig. 1 we represent a schematic 2D log-log map indicating these two lines defining the crest, in two different positions inside the experimental window defined by $A_{\min}$, $A_{\max}$, $T_{\min}$, and $T_{\max}$. In the inset we also show the behavior of the function $g(Z)$ in log-log scale and the position of the values Z_0 (maximum), Z_A (with slope $-\gamma$), and Z_T (with slope δ/x) for a case $x>0>-\gamma>\delta/x$. Note that the position and the smoothness of the crest is related not only to Z_0 but also to the exponents γ, δ, and x. We can guess the position of the crest around $Z_c=(Z_A+Z_T)/2$. Although Z_c does not need to be close to Z_0, once the signs of the exponents γ, δ, and x are fixed, the position of Z_0 should be compatible with the picture shown in the inset of Fig. 1, i.e., for the case $x>0>-\gamma>\delta/x$ the following inequality holds: $Z_0<Z_A<Z_c<Z_T$.

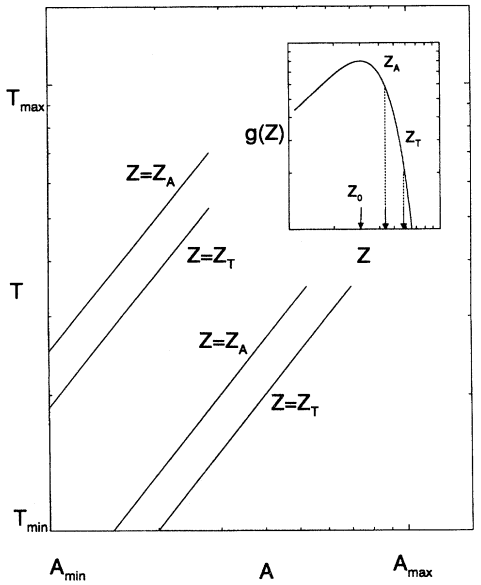

FIG. 1. Schematic diagram of the behavior of the crest of the joint distribution inside the experimental window.

In order to fit the distribution given by Eq. (13) to the histograms obtained from experimental data, the first point to consider is the experimental window. Since we are dealing with decaying power-law behaviors, the experimental upper cutoffs at $A_{\max}$ and $T_{\max}$ do not usually represent a problem for the interpretation of the data. In practice, the actual upper cutoffs will be determined by the lack of statistics. For the lower cutoffs one should distinguish the two possibilities shown in Fig. 1. If $Z_c\simeq Z_A\simeq Z_T\ll Z_{\lim}$ with $Z_{\lim}=A_{\min}/T_{\min}^x$, the marginal distributions $p(A)$ will not be distorted by the window, but $p(T)$ will exhibit a bend for $T<(A_{\min}/Z_c)^{1/x}$. On the contrary, if $Z_c\simeq Z_A\simeq Z_T\gg Z_{\lim}$, $p(T)$ will not be distorted but $p(A)$ will exhibit the bend for $A<T_{\min}^x Z_c$.

III. DISTRIBUTION FUNCTION FITTING

As an example of the usefulness of the model proposed above we use it, in this section, to describe the distribution of acoustic emission signals in thermally induced martensitic transformations (Part I). We will analyze separately data corresponding to the forward (cooling) and reverse (heating) transformations. As discussed in the previous paper, the experimental window is defined by $A_{\min}=4\times10^{-4}$ V, $A_{\max}=5\times10^{-3}$ V, $T_{\min}=10^{-5}$ s, and $T_{\max}=5\times10^{-4}$ s.

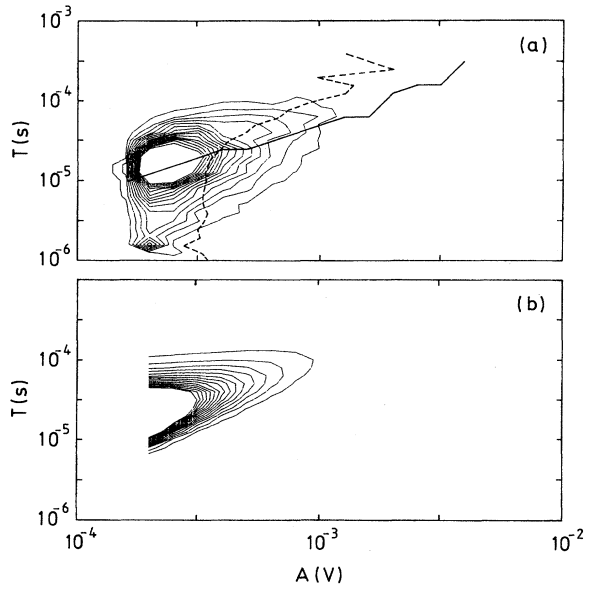

FIG. 2. Comparison of the experimental joint distribution map (a) with the theoretical fit (b) for cooling. The lines in the upper figure correspond to $\langle A|T\rangle$ and $\langle T|A\rangle$ defined in Eqs. (16) and (17).

Figures 4 and 5 of part I show the log-log plots of the histograms corresponding to the marginal distributions $p(A)$ and $p(T)$ for AE signals recorded during cooling and heating. Note that the window effect is clearly observed in the distribution of durations $p(T)$, which shows a bend at $T\sim 8\times 10^{-5}$ s, a value much higher than $T_{\min}$ expected from the experimental window. For the sake of comparison to the present model, in Figs. 2(a) and 3(a) we show the map of the 2D histogram of the experimental data in log-log scale for

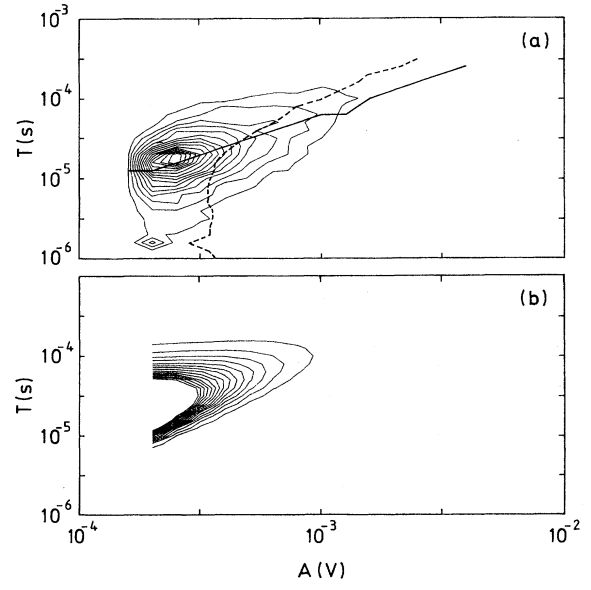

FIG. 3. Comparison of the experimental joint distribution map (a) with the theoretical fit (b) for heating. The lines in the upper figure correspond to $\langle A|T\rangle$ and $\langle T|A\rangle$ defined in Eqs. (16) and (17).

cooling and heating, respectively. They have been obtained using logarithmic bins of size 0.1 decades in both magnitudes A and T. The behavior of the crests can be estimated by joining the points of maximum curvature of the contour levels of the distributions. They roughly follow a line with slope $x\sim 1$ and a value $Z_c\sim 10$ V/s for both cooling and heating. Considering $x=1$, the experimental window margins result in a value of $Z_{\lim}=A_{\min}/T^x_{\min}=40$ V/s. Therefore, in this case $Z_c<Z_{\lim}$ and we could expect an undistorted $p(A)$ and the occurrence of a bend in $p(T)$ around $(A_{\min}/Z_c)^{1/x}=4\times 10^{-5}$ s. This value is close to the actual position of the bend.

As detailed in part I, by least-squares fitting to the marginal distribution one can obtain $\alpha=3.8\pm 0.8$ and $\tau=3.6\pm 0.8$ for cooling and $\alpha=3.5\pm 0.8$ and $\tau=3.5\pm 0.8$ for heating. These values render [through relation (10)] an exponent $x=1.0\pm 0.5$ for both cooling and heating, consistent with the behavior of the crest observed in the log-log map of the joint distribution [Figs. 2(a) and 3(a)]. An independent method for the estimation of x is to use any of the conditional mean values of T for a given A or A for a given T, defined as

$$\langle T|A\rangle=\int_{T_{\min}}^{T_{\max}} T\,\frac{p(A,T)}{p(A)}\,dT\sim A^{1/x}\ , \tag{16}$$

$$\langle A|T\rangle=\int_{A_{\min}}^{A_{\max}} A\,\frac{p(A,T)}{p(T)}\,dA\sim T^{x}\ . \tag{17}$$

These are easy-to-compute alternatives to the two equations (14) and (15). Usually the estimation of the maximum of a function is noisier and less accurate than the estimation of the mean value. The conditional mean values are shown in Figs. 2(a) and 3(a) on top of the maps of the experimental joint distributions for cooling and heating, respectively. The continuous line represents $\langle T|A\rangle$ while the dashed line represents $\langle A|T\rangle$. The results are compatible with the power-law behaviors in Eqs. (16) and (17). The breakdown of the power-law behavior of $\langle A|T\rangle$ for small values of T is due the window effect explained above. A fit to $\langle T|A\rangle$ renders $x=1.0\pm 0.1$ for both heating and cooling. This value is compatible with the behavior of $\langle A|T\rangle$ for $T>8\times 10^{-5}$ s.

After completion of the fit of the marginal distributions, and given the exponent relations (11) and (12), we should fit compatibly the function $g(A/T^x)$ defined in (13). Since the 2D fitting is often difficult and less stable, it is better to use a 1D projection of the function g. To do so, we calculate the marginal distribution of $Z=A/T^x$ defined as

$$p(Z)dZ=\int_{A_{\min}}^{A_{\max}}\int_{T_{\min}\,Z=\text{const}}^{T_{\max}} p(A,T)\,dA\,dT\ . \tag{18}$$

By changing the variables of the joint distribution from (A,T) to $(Z=A/T^x,T)$, integrating over T and taking into account the window effect, one obtains

$$p(Z)dZ\sim\begin{cases} g(Z)\ Z^{\gamma}\ Z^{\tau-1/x} & \text{for } Z<Z_{\lim} \\ g(Z)\ Z^{\gamma} & \text{for } Z>Z_{\lim}\end{cases}\ . \tag{19}$$

Assuming $x=1$, we have tried a number of distribution functions for $g(Z)$ (Gaussian, Laplace, extreme-value, etc.) in

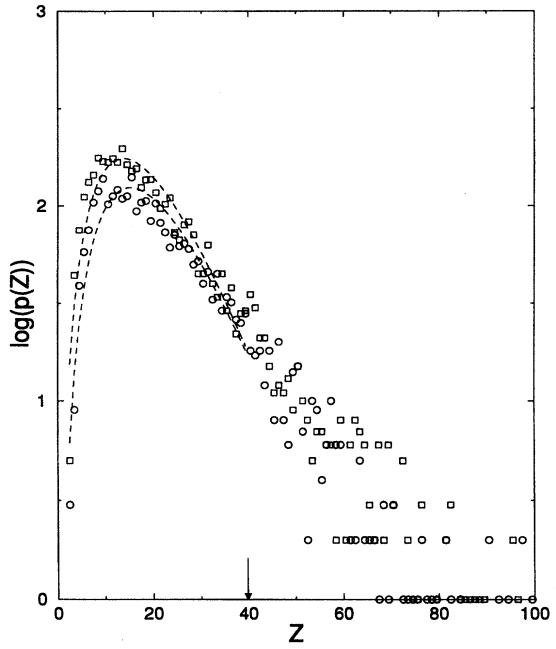

FIG. 4. Distribution $p(Z)$ on a $\log_{10}$ scale as defined in Eq. (18) for cooling (circles) and heating (squares). Solid lines are best fits performed using an extreme value distribution defined by Eq. (20) for $Z<Z_{\rm lim}=40$ V/s (indicated by the arrow).

order to fit the experimental distribution $p(Z)$ shown in Fig. 4 in the region $Z<Z_{\rm lim}$. All the fitted functions, in addition to the exponent γ, had three parameters, namely the position of the maximum (Z_0), the width c and the height of the peak. The best fit to $\ln p(Z)$, consistent with the model, has been obtained for an extreme-value distribution of the form:

$$g(Z)=\frac{1}{c}\exp\left[-\frac{Z-Z_0}{c}-e^{-Z-Z_0/c}\right] , \qquad (20)$$

with $\gamma=0.0\pm1.0$, $\delta=-4.7\pm1.0$, $c=5.3\pm1.0$ V/s, and $Z_0=0.26\pm0.10$ V/s for cooling, and $\gamma=0.2\pm1.0$, $\delta=-4.5\pm1.0$, $c=5.2\pm1.0$ V/s, and $Z_0=3.4\pm1.0$ V/s for heating. This fit gives values $\chi^2=0.53$ and $\chi^2=0.57$ for cooling and heating, respectively. The values of Z_0 are clearly below $Z_{\rm lim}=40$ V/s consistent with the values of the exponents γ and δ, as discussed in the previous section. It should be mentioned that a fit to a Gaussian distribution rendered smaller values $\chi^2=0.18$ and $\chi^2=0.3$ for cooling and heating, respectively; nevertheless such a fit is not acceptable because it provided $\gamma\simeq2.3>0$, $\delta\simeq-7<0$ and a value $Z_0\simeq55$ V/s$>Z_{\rm lim}$. This value results in a still higher Z_c, in clear disagreement with the position of the crest ($Z_c\sim10$ V/s) in Figs. 2(a) and 3(a). In fact the 2D plot of the Gaussian fit was quite different from the experimental histogram, but this disagreement was hidden in the 1D projection $p(Z)$, rendering the small value of χ^2. It is always convenient to directly compare the 2D plots of the model to the experimental maps. Figures 2(b) and 3(b) show the 2D-maps of the final joint distributions obtained from the best fits. The same contour levels have been used for the experimental and theoretical maps. The agreement is quantitatively satisfactory for large enough A and T. For low values of A and T, the experimental 2D map shows the existence of two peaks: the large one, on the top, is an artifact arising from the experimental window, and the lower one comes from electric noise.

There might be a physical explanation for the extreme value distribution of the variable $Z=A/T$, based on the fact that the amplitude measured in the AE experiments is the maximum value of the signal (which might well be distorted by Gaussian fluctuations). These constants c and Z_0, and the exponents γ and δ are related to the most probable A/T relation of a signal and should depend on the sample properties. A definite explanation for this point will only be possible when the connection between the acoustic emission and the physics of the transformation in the sample is well understood.

A summary of the fitted exponents consistent with the analysis of the data is presented in Table I. Although we have found slightly different values for cooling and heating, the error bars do not allow to assert that such differences are physically meaningful.

TABLE I. Summary of the exponents characterizing the joint distribution of AE signals.

x	α	τ	ϕ	γ	δ
1.0 ± 0.1	3.6 ± 0.8	3.5 ± 0.8	0.9 ± 0.1	0.1 ± 1.0	-4.6 ± 1.0

IV. CORRELATION FUNCTION MODELING

In this section we study the time correlation function of signals distributed according to the model presented in Sec. II. In order to calculate it we need an hypothesis on the shape of the signals characterizing each avalanche. The simplest choice is to assume that each AE signal has square shape.[11] Thus, the full recorded AE trains are a superposition of square individual signals, i.e.,

$$\Psi(t)=\sum_{i=1}^{M}\psi(A_i,T_i,t-t_i) , \qquad (21)$$

where

$$\psi(A_i,T_i,t-t_i)=\begin{cases}0 & \text{for } t<t_i,\\ A_i & \text{for } t_i<t<t_i+T_i,\\ 0 & \text{for } t>t_i+T_i\end{cases} \qquad (22)$$

being M the total number of signals between $t=0$ and $t=\Delta$. The complete train $\Psi(t)$ is then characterized by the set of $3M$ random variables $\{A_i,T_i,t_i\}$. At this point, we make an independence hypothesis, i.e., we assume that the probability of a given set of the $3M$ variables can be factorized like

$$p(A_1,A_2,\cdots A_M,T_1,T_2,\cdots T_M,t_1,t_2,\cdots,t_M)=\prod_{i=1}^{M}\left(p(A_i,T_i)\frac{1}{\Delta}\right). \qquad (23)$$

With this assumption, the average $\langle c(t)\rangle$ over a set of trains of the correlation function defined by

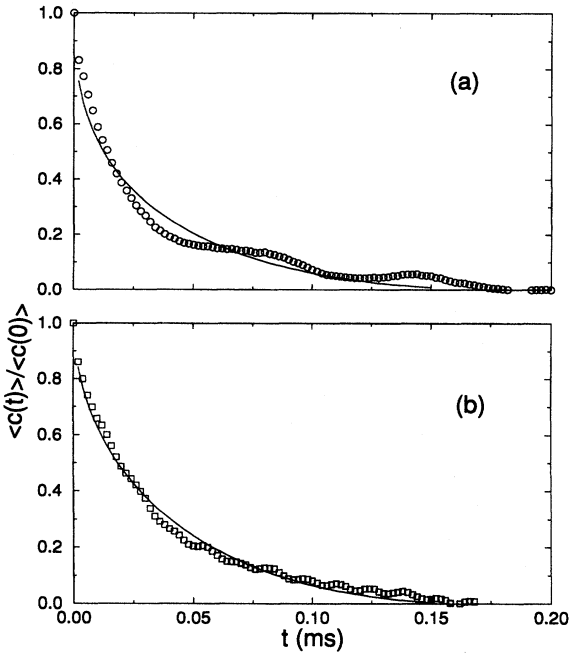

FIG. 5. Time correlation function for cooling (a) and heating (b). The lines are fits of Eq. (27).

$$c(t)=\frac{1}{\Delta}\int_0^{\Delta}\Psi(u)\Psi(t+u)\,du-\left(\frac{1}{\Delta}\int_0^{\Delta}\Psi(u)\,du\right)^2 , \tag{24}$$

reduces to the average autocorrelation of the individual signals:

$$\langle c(t)\rangle=M\left\langle\frac{1}{\Delta}\int_0^{\Delta}\psi(u)\psi(t+u)\,du-\left(\frac{1}{\Delta}\int_0^{\Delta}\psi(u)\,du\right)^2\right\rangle . \tag{25}$$

By integration it can easily be shown that, for the square signals defined by (22), the above equation can be written as

$$\langle c(t)\rangle=\frac{M}{\Delta}\left(\langle A^2(T-|t|)\,\theta(T-|t|)\rangle-\frac{1}{\Delta}\langle A^2T^2\rangle\right) , \tag{26}$$

with M/Δ being the mean frequency of the avalanches. According to the model proposed in Sec. II, the second term $(1/\Delta)\langle A^2T^2\rangle$ of the correlation function represents an integral over A and T inside the window limited by $A_{\min}$, $A_{\max}$, $T_{\min}$, and $T_{\max}$. In principle, $T_{\max}$ might be as large as Δ, rendering a long-time nonvanishing correlation function.[12] Nevertheless, in most cases the lack of statistics may introduce a cutoff $T_{\max}\ll\Delta$ which makes the second term negligible. Thus, neglecting this second term, given the distribution $p(A,T)$ from Eq. (13) and assuming $x=1$ one gets

$$\frac{\langle c(t)\rangle}{\langle c(0)\rangle}=1-\frac{4-\tau}{3-\tau}\frac{|t|}{T_{\max}}+\frac{1}{3-\tau}\left(\frac{|t|}{T_{\max}}\right)^{4-\tau} . \tag{27}$$

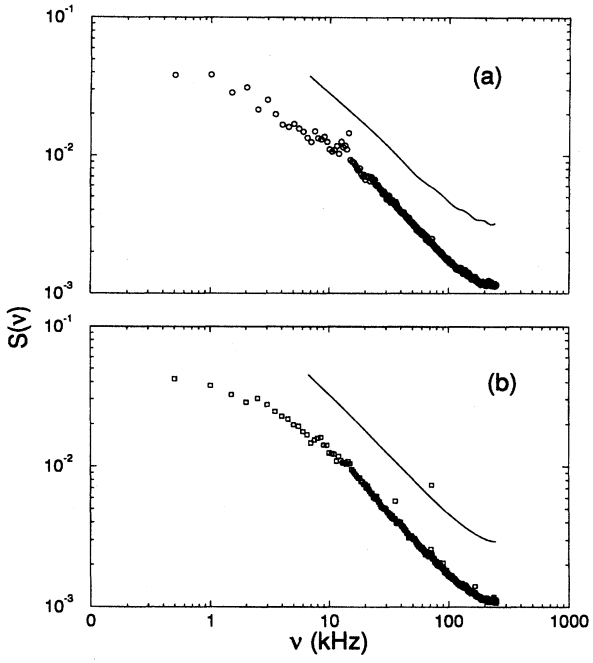

FIG. 6. Power spectrum calculated by Fourier transforming data from Fig. 8. The lines are the Fourier transforms of the corresponding fits.

V. CORRELATION FUNCTION AND POWER SPECTRUM FITTING

Again, we compare the correlation function (27) obtained from our model to the AE experiments in martensitic transformations. The available experimental data consist of a set of 20 long trains recorded at 0.5 MHz and lasting for 16 ms. The correlation function is obtained by computing numerically the individual correlation functions corresponding to each train, and then averaging over the set of trains. By least-squares fitting expression (27) one obtains the values $\tau=3.6\pm0.4$, $T_{\max}=0.19\pm0.2$ ms for cooling and $\tau=3.4\pm0.4$, $T_{\max}=0.17\pm0.2$ ms for heating. The fits are shown on top of the experimental data in Figs. 5(a) and 5(b), respectively. The values obtained are estimations of the exponent τ independent of the previous values obtained from the marginal distributions, presented in Sec. II. The agreement is excellent. The values obtained for $T_{\max}$ are smaller than those defined in Sec. II, since the statistics in the acquisition of long trains is poorer than the statistics in the acquisition of single AE signals. In fact, this value is of the order of the length of the largest recorded signals in a train. The Fourier transforms of the fitted functions are plotted in Figs. 6(a) and 6(b) and compared with the experimental power spectrum. Both curves show an intermediate region with a behavior compatible with $S(\nu)\sim\nu^{-\phi}$, with $\phi\simeq0.9\pm0.1$. Thus, our model also provides a description for the $1/f$ noise observed in the experiments.

In order to compare with existing results in the literature[11] we have calculated the function $\Lambda(T)$, defined as

$$\Lambda(T)=T^2\int_{A_{\min}}^{A_{\max}}A^2p(A,T)\,dA . \tag{28}$$

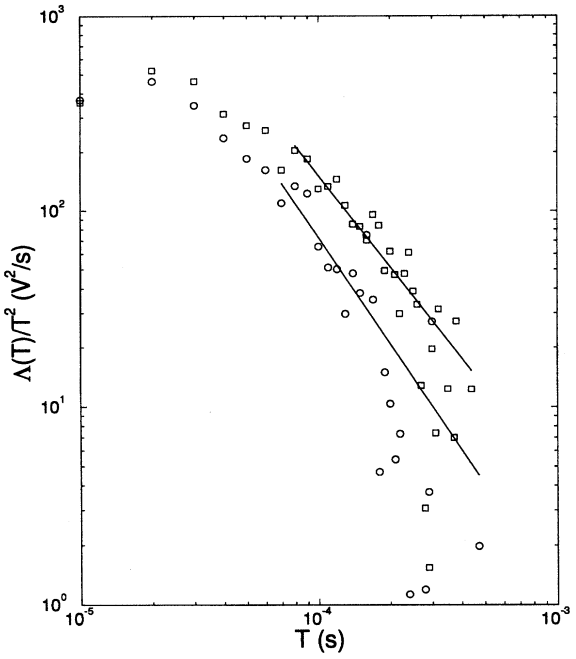

FIG. 7. Log-log plot of the function $\Lambda(T)/T^2$ as defined in the text for cooling (circles) and heating (squares). The lines are power-law fits with slopes $\mu-2=0.2\pm0.6$ and $\mu-2=0.4\pm0.6$, respectively.

Figure 7 shows $\Lambda(T)/T^2$ for cooling and heating. By least squares fitting to the log-log data we have obtained the slopes $\mu-2=-1.8\pm0.6$ for cooling and $\mu-2=-1.6\pm0.6$ for heating, giving a power-law dependence $\Lambda(T)\sim T^{\mu}$ with $\mu\simeq0.3\pm0.6$. This value is in agreement with the theoretical value $\mu=4-\tau=0.5\pm0.6$ computed using the fitted $p(A,T)$ from Eq. (13). Christensen *et al.*[11] propose that the exponent of the power spectrum ϕ should satisfy the relation $\phi=\mu+1$. This gives an estimation $\phi=1.3\pm0.6$ which should be compared with the value from the experimental power spectrum $\phi=0.9\pm0.1$. The agreement is roughly correct. Nevertheless, the assumption of Christensen *et al.* that the behavior of the autocorrelation function of the individual signals is characterized only by the exponents of its power behavior at very high and very low frequencies turns out to be too simplified for AE in martensitic transformations, for which the behavior of the autocorrelation of each signal at intermediate frequencies plays a significant role in the power spectrum.

VI. CONCLUSIONS

The first conclusion of the paper is the usefulness of the description of the statistics of the avalanches by the joint distribution function. We have designed a phenomenological model, based on scaling arguments, describing the exponents characterizing the power-law marginal distribution and the statistical dependence $A\sim T^x$ found in different experiments on avalanches.

For the AE signals in martensitic transformations we have fitted the above model. After correction of the effects due to the experimental window, we have obtained the full set of exponents α, τ, x, δ, and γ shown in Table I, together with the constants Z_0 and c accounting for the most probable value and the dispersion of the ratio A/T. The model has also been useful in understanding the correlation function and the power spectrum of such AE signals. Our results are compatible with the assumption of independence of the individual signals in a train. We have also found a theoretical function (27) which reproduces the power spectrum in two decades, from 3 to 300 kHz. This function gives the $1/f$ behavior observed in an intermediate range (10–100 kHz) of frequencies.

ACKNOWLEDGMENTS

We acknowledge A. Planes, J. Ortín, and Ll. Mañosa for fruitful comments. We also acknowledge financial support from CICyT (Spain), Project No. MAT92-884.

[1] P. Bak, C. Tang, and K. Wiesenfeld, Phys. Rev. Lett **59**, 381 (1987); Phys. Rev. A **38**, 36 (1988).

[2] P. Diodati, F. Marchesoni, and S. Piazza, Phys. Rev. Lett. **67**, 2239 (1991); C. F. Richter, in *Elementary Seismology* (Freeman, San Francisco, 1959); L. Knopoff, in *Disorder and Fracture*, edited by J. C. Charmet, S. Roux, and E. Guyon (Plenum, New York, 1990), p. 279; D. Sornette, in *Proceedings of Spontaneous Formation of Space-time Structures and Criticality*, edited by T. Riste and D. Sherrington (Kluwer Academic, Dordrecht, 1991), p. 57.

[3] W. Wu and P. W. Adams, Phys. Rev. Lett. **74**, 610 (1995).

[4] K. L. Babcock and R. M. Westervelt, Phys. Rev. Lett. **64**, 2168 (1990).

[5] P. J. Cote and L. V. Meisel, Phys. Rev. Lett. **67**, 1334 (1991); L. V. Meisel and P. J. Cote, Phys. Rev. B **46**, 10 822 (1992).

[6] G. A. Held, D. H. Solina II, D. T. Keane, W. J. Haag, P. M. Horn, and G. Grinstein, Phys. Rev. Lett. **65**, 1120 (1990).

[7] M. Bretz, J. B. Cunningham, P. L. Kurczynski, and F. Nori, Phys. Rev. Lett. **69**, 2431 (1992).

[8] G. Cannelli, R. Cantelli, and F. Cordero, Phys. Rev. Lett. **70**, 3923 (1993).

[9] E. Vives, J. Ortín, Ll. Mañosa, I. Ràfols, R. Pérez-Magrané, and A. Planes, Phys. Rev. Lett. **72**, 1694 (1994).

[10] M. P. Lilly, P. T. Finley, and R. B. Hallock, Phys. Rev. Lett. **71**, 4186 (1993).

[11] K. Christensen, H. C. Fogedby, and H. J. Jensen, J. Stat. Phys. **63**, 653 (1991); H. J. Jensen, K. Christensen, and H. C. Fogedby, Phys. Rev. B **40**, 7425 (1989).

[12] The assumption of a power-law distribution up to $T_{\max}\sim\Delta$ for the durations of the signals implies that the correlation function does not go to zero for long times but depends on the duration of the measurements.